MNRAS **000**, 1–19 (2016) Preprint 15 July 2016 Compiled using MNRAS LATEX style file v3.0

The origin of the excess transit absorption in the HD 189733 system: planet or star?

J.R. Barnes[1], C.A. Haswell[1], D. Staab[1], G. Anglada-Escudé[2],
[1] *Department of Physical Sciences, The Open University, Walton Hall, Milton Keynes MK7 6AA, UK.*
[2] *School of Physics and Astronomy, Queen Mary, University of London, 327 Mile End Rd. London, UK*

arXiv:1607.03684v2 [astro-ph.EP] 14 Jul 2016

Received May 2016; Accepted for publication July 2016

ABSTRACT

We have detected excess absorption in the emission cores of Ca II H & K during transits of HD 189733b for the first time. Using observations of three transits we investigate the origin of the absorption, which is also seen in Hα and the Na I D lines. Applying differential spectrophotometry methods to the Ca II H and Ca II K lines combined, using respective passband widths of $\Delta\lambda = 0.4$ & 0.6 Å yields excess absorption of $t_d = 0.0074 \pm 0.0044$ (1.7σ; Transit 1) and 0.0214 ± 0.0022 (9.8σ; Transit 2). Similarly, we detect excess Hα absorption in a passband of width $\Delta\lambda = 0.7$ Å, with $t_d = 0.0084 \pm 0.0016$ (5.2σ) and 0.0121 ± 0.0012 (9.9σ). For both lines, Transit 2 is thus significantly deeper. Combining all three transits for the Na I D lines yields excess absorption of $t_d = 0.0041 \pm 0.0006$ (6.5σ). By considering the time series observations of each line, we find that the excess apparent absorption is best recovered in the stellar reference frame. These findings lead us to postulate that the main contribution to the excess transit absorption in the differential light curves arises because the normalising continuum bands form in the photosphere, whereas the line cores contain a chromospheric component. We can not rule out that part of the excess absorption signature arises from the planetary atmosphere, but we present evidence which casts doubt on recent claims to have detected wind motions in the planet's atmosphere in these data.

Key words: (stars:) planetary systems stars: activity stars: atmospheres stars: chromospheres techniques: spectroscopic

1 INTRODUCTION

Appropriately, the first known transiting exoplanet, HD 209458b (Charbonneau et al. 2000; Henry et al. 2000), also yielded the first detection of an atmosphere outside the solar system. The excess absorption of $(2.32\pm0.57)\times10^{-4}$ in the 5893 Å Na resonance doublet compared with neighbouring continuum passbands suggested that Na was present at a lower level than predicted (Seager & Sasselov 2000). Clouds, hazes and photo-ionisation of Na were investigated by Seager (2003), Fortney et al. (2003) and Barman (2007) as possible causes for the low observed Na absorption. A complete optical transmission spectrum of HD 209458b spanning 3000 - 7000 Å was observed for the first time with the Hubble Space Telescope (HST), additionally revealing strong Rayleigh scattering (Lecavelier Des Etangs et al. 2008) at wavelengths of 3000 - 5000 Å. With a later spectral type of K1V - K2V, HD 189733 causes lower incident radiation of the orbiting hot Jupiter despite its smaller orbital radius. HST transmission spectroscopy of HD 189733b have revealed that Na is observed as a weak feature (Pont et al. 2008, 2013) while strong Rayleigh scattering dominates at shorter optical and UV wavelengths (Pont et al. 2008; Sing et al. 2011; Pont et al. 2013).

Ground-based transmission spectroscopy of transiting exoplanets is notoriously difficult owing to the small signal and variable nature of the Earth's atmosphere. When spectroscopy is employed, variable seeing changes the slit and hence grating illumination, leading to systematic changes in the recorded spectrum. These are generally second order effects, but are crucial when searching for precision radial velocity signatures or subtle changes in the spectrum at levels of order a few per cent or less. Spectrophotometry has proven to be one successful method enabling multi-wavelength transit radius measurements in the atmospheres of close orbiting planets. For example, Sing et al. (2012) used a wide 5″ long slit to carry out differential spectrophotometry of the planet hosting star, XO-2A, and its planet, XO-2b, yielding a 5.2-σ detection of Na.

Extending ground-based characterisation to higher resolution is clearly desirable if we wish to detect individual transitions and measure abundances in detail. Échelle

© 2016 The Authors

Table 1. HARPS observations during transit of HD 189733b. Columns 5-9 list S/N ratios for the Ca II H & K, the mean of the nearby Mount Wilson S index V & R continuum passbands, Hα and the mean of the Hα A & B continuum passbands.

					Passband S/N ratios				
	Date	Seeing ($''$)	Exptime (s)	Airmass	Ca II K	Ca II H	$\overline{V+R}$	Hα	$\overline{A+B}$
Transit 1	2006/09/07	0.85 ± 0.22	600 - 900	2.1 - 1.6	21.4	28.0	28.3	91.0	162.4
Transit 2	2007/07/19	0.68 ± 0.11	300	2.4 - 1.6	14.6	18.6	19.8	57.8	106.1
Transit 3	2007/08/28	1.17 ± 0.51	300	2.3 - 1.6	12.5	16.5	16.9	52.8	94.7

spectroscopy offers the wavelength range needed, but with many optical components, including a grating and a cross-disperser, this presents greater challenges, especially when narrow slit widths of typically $\lesssim 1''$ are commonly employed. Fibre fed instruments offer the best internal stability since the light is largely scrambled by the fibre and hence the illumination of the slit on exit from the fibre is less sensitive to seeing changes and guiding errors. By normalising each observation to nearby continuum regions, excess absorption in individual lines can be probed. This was first applied specifically to HD 189733b by Redfield et al. (2008) to detect excess Na absorption during transit and more recently using data from the High Accuracy Radial Velocity Planet Searcher (HARPS) by Wyttenbach et al. (2015). Louden & Wheatley (2015) have also applied a model that accounts for the differences in the Doppler shift of absorption from opposite sides of the planet. The planetary absorption line profiles were thus modelled as a function of time during the transit to infer an equatorial eastward jet in the planet's atmosphere.

Fossati et al. (2013) hypothesised that extrinsic absorbing gas local to the WASP-12 system and arising from WASP-12b is responsible for the anomalously low flux in the Ca II H & K cores of WASP-12. If gas is uniformly distributed around the star, we would expect the absorption to be constant with time. Fossati et al. (2010) and Haswell et al. (2012) showed that there is more near ultraviolet absorption around the phases of transit, so the absorbing gas in the WASP-12 system is densest there. Because WASP-12 is faint, and there is very little flux in the line cores (Fossati et al. 2013), we decided to study HD 189733b to search for time variable Ca II H & K absorption. HD 189733 is a K1.5V star with a relatively small radius of $R_* = 0.756 \pm 0.018$ $R_\odot$ (Torres et al. 2008). Hence a large transit signature for a given planet radius is expected compared with a star such as WASP-12b with an estimated radius of $R_* = 1.6$ $R_\odot$. Conversely, the pressure scale height of $H_{eq} = 201$ km is not particularly high compared with HD 209458b, with $H_{eq} = 553$ km (Sing et al. 2016).

In this paper, we examine Ca II H & K and Hα absorption during the transit of HD 189733b. We also re-examine Na I D1 & D2 absorption following a recent analysis by Wyttenbach et al. (2015) and also use the Ca I 6122 Å line as a control. The archival HARPS data exhibit clear evidence of excess absorption during transit, thanks largely to the fact that the star is active and hence exhibits Ca II H & K cores with sufficient flux to reliably detect the transit. In §2, we discuss the activity and chromospheric variability of HD 189733. The observations and the methods used to derive the transit light curves is presented §3. We present the transit light curves in §4 and the residual line profiles during transit in §5. We discuss the possible origin of the excess absorption during transit in light of our finding that the absorption is both variable and more sharply defined in the stellar reference frame than the planet reference frame §6. A summary and concluding remarks are found in §7.

2 CHROMOSPHERIC AND PHOTOSPHERIC VARIABILITY OF HD 189733

The relatively active nature of HD 189733 was recognised in the discovery paper by Bouchy et al. (2005), following measurements of the Mount Wilson S index by Wright et al. (2004). During the observations studied here, the S index (Vaughan et al. 1978), varies in the range 0.461 to 0.508, with associated R'_{HK} (Noyes et al. 1984) values in the range $-4.55 \leq \log R'_{HK} \leq -4.50$. For comparison, the Sun typically shows average values of $-5.0 \leq \log R'_{HK} \leq -4.85$ for solar minimum and solar maximum periods (Lagrange et al. 2010).

Active stars also exhibit greater chromospheric variability than less active stars, as seen when comparing S indices measured in the same stars at different epochs (Wright et al. 2004; Jenkins et al. 2006). Variability may result from stellar magnetic cycles, rotational modulation or shorter lived transients such as flares. Shkolnik et al. (2003) found evidence for synchronous enhancement of Ca II H & K in HD 179949 due to its non-transiting hot Jupiter. In contrast, modulation only at the rotation period of HD 189733 was found by (Shkolnik et al. 2008). Similarly, Boisse et al. (2009) found periodicity in the Ca II H & K lines close to the stellar rotation period of HD 189733.

The chromospheric activity variability complicates both radial velocity measurements and transit measurements. Boisse et al. (2009) used correlations between chromospheric indicators and radial velocity measurements to improve their orbital solution, and hence the mass estimate of HD 189733b. Since photospheric distortions from associated cool starspots are the main cause of astrophysical noise in high precision stellar radial velocities, their effects must also be accounted for, particularly where high S/N ratio space-based observations that are free from atmospheric systematics are available. Both Pont et al. (2008) and Sing et al. (2011) have included spot modelling analysis in precision transmission spectroscopy with Hubble Space Telescope observations of HD 189733b, to obtain improved estimates of wavelength-dependent transit depths.

In addition to the problems introduced by chromospheric variability, throughput efficiency typically declines in spectrometers at blue wavelengths. For HARPS the effi-

ciencies at 3800 Å and 4000 Å are respectively 0.24 and 0.47 of its maximum throughput of 5.7 per cent[1]. The S/N ratios achievable in the cores of the strong Ca II H & K lines are thus generally low as the typically low throughput of the instrument is exacerbated by the deep photospheric absorption in these features. Hence, stars exhibiting moderate activity, and thus appreciable line core emission flux, are likely to offer the best chances of detecting a planetary transit in Ca II H & K, providing that the star remains relatively quiet during and around transit. A recent study of HD 189733b by Czesla et al. (2015), utilising UVES/VLT observations has investigated the limb-darkening effect during transit in the Na doublet and Ca II H & K lines, but the cores of the lines, particularly Ca II H & K, were affected by a flaring event.

3 OBSERVATIONS AND DIFFERENTIAL SPECTROPHOTOMETRY

HD 189733b has been observed with HARPS during a number of transit events[2]. The HARPS Data Reduction Software (DRS) does not apply background subtraction of scattered light. We find that after bias subtraction, the typical line core fluxes for Ca II H, Na I D1 and Hα include respective scattered light components of 1.3, 2.9 and 0.3 per cent. Instead of using the standard DRS, we re-extracted the data using a new extraction pipeline. This is based on the Flat-ratio Optimal eXtraction (FOX) demonstrated in Zechmeister et al. (2014). Prior to the FOX extraction, special care is take in performing a detailed background subtraction. This can be important in regions where few counts are obtained, such as the cores of strong lines that contain little flux. That is, all the fibre A and B traces containing the science and simultaneous calibration spectra are set to zero weight and a 2-dimensional 3rd-degree polynomial fit is done on both HARPS chips to remove the smooth component of the background. This still leaves small residuals, especially on the edges of the detector and regions contaminated by secondary ghost spectra produced by HARPS. To mitigate these, each pixel column (cross-dispersion, science and calibration spectra still blocked) is also fitted to a parabola and subtracted.

Since the fraction of scattered light is greatest in the line cores, any further flux deficit during transit will be more significant in the case where the scattered light is removed during extraction. This will lead to greater transit depth measurements. The transits we measure in §4 are ~ 2.5 per cent deeper for Ca II H & K and Na I D1 & D2 using our extraction compared with the DRS spectra. We note that the significance of this finding is nevertheless at a level lower than our measurement uncertainties.

We use the same naming scheme as Wyttenbach et al. (2015) who studied transits of the Na line using the same data. Transit 1 data were obtained on 2006/09/07 with exposure times between 600 secs and 900 secs. Transit 2 and 3 data were taken on 2007/07/19 and 2007/08/28 respectively, with 300 sec exposures. In Table 1, we summarise the observations, and give S/N ratios for the Ca II H & K, and Hα regions considered in this paper. Column 4 of Table 1 shows that the observations were made at high airmass owing to the northerly declination ($\delta = 22.6°$). The seeing recorded in the observation FITS headers indicates variable conditions at each epoch. Column 3 of Table 1 shows that the best seeing was present during Transit 2 ($0.68''$), which also afforded the most stable conditions. The seeing during Transit 3, with a mean of $1.17''$, was substantially worse. Since the HARPS fibres are $1''$ on sky, we expect the most efficient and stable spectra to have been observed during Transit 2.

Atmospheric variability generally precludes precision flux measurements with spectrometers fed by a slit of comparable width to the seeing PSF. The accuracy required can nevertheless be achieved by self-calibrating the spectrum using simultaneous differential measurements. Using this method, Charbonneau et al. (2002) made differential measurements of the Na lines by comparing in-transit (IT) and out-of-transit (OOT) fluxes centred on Na with those in neighbouring continuum bands. This is a doubly differential method: the difference between IT and OOT and the difference between the line and continuum is considered. It can only be used to reliably infer absorption from the planet atmosphere if the stellar spectrum is completely constant with time. This approach has been adopted by a number of authors including Wyttenbach et al. (2015), who applied it to the HARPS observations we use here. In this way, the signature of continuum light blocked by the opaque planet is removed. With no wavelength-dependent signal (i.e. additional line absorption relative to the continuum) we thus expect no sign of transit, while excess absorption during IT phases can be attributed to the presence of a line in the planetary atmosphere.

3.1 Transit light curve measurement of Ca II H & K lines

The differential transit light curve method is analogous to the Mount Wilson method of measuring Ca II H & K: the S index combines both H & K line core fluxes to improve the S/N ratio (see Table 1). Here we consider the fractional flux in the Ca II H & K lines relative to the nearby continuum bands. The unweighted line core flux, $\mathscr{U}_{HK}(t)$, for an observation at time, t, can be written as

$$\mathscr{U}_{HK}(t) = \frac{\overline{K}(t) + \overline{H}(t)}{\overline{V}(t) + \overline{R}(t)} \quad (1)$$

where $\overline{K}(t)$ and $\overline{H}(t)$ are the mean fluxes in passbands centred on the Ca II K and Ca II H lines respectively. Similarly, the blue continuum band flux is $\overline{V}(t)$ and the red continuum band flux is $\overline{R}(t)$. We stress that the line fluxes are *not* the same as the Mount Wilson fluxes which are weighted with a triangular passband (Vaughan et al. 1978) of width 1.09 Å. The exact width of the H & K passbands are however important, and should include the wavelength range

[1] http://www.eso.org/sci/facilities/lasilla/instruments/harps/doc.html

[2] This work is based on observations collected at the European Organisation for Astronomical Research in the Southern Hemisphere under ESO programmes 072.C-0488(E), 079.C-0127(A) and 079.C-0828(A). The data are available at https://archive.eso.org.

over which any IT vs OOT transit variability is seen. Although the overall flux in H is lower than in K, the S/N ratio in H is higher, as indicated in Table 1. We therefore optimally add the mean fluxes according to their associated variances, $\overline{\sigma_H}^2$ and $\overline{\sigma_K}^2$, which are calculated from the individual pixel variances. Hence, for our analysis by replacing the numerator, $\overline{K}(t) + \overline{H}(t)$ in Equation 1 with

$$\overline{HK}(t) = \frac{\overline{K}(t)/\overline{\sigma_K}^2(t) + \overline{H}(t)/\overline{\sigma_H}^2(t)}{1/\overline{\sigma_K}^2(t) + 1/\overline{\sigma_H}^2(t)} \quad (2)$$

We can thus write the combined, weighted Ca II H & K line core flux, as

$$\mathscr{F}_{HK}(t) = \frac{\overline{HK}(t)}{\overline{V}(t) + \overline{R}(t)} \quad (3)$$

The V and R band fluxes are not optimally added, as this may introduce airmass-dependent normalisation systematics. This is especially important as altitude dependent atmospheric refraction is a steep function at blue wavelengths.

The mean S/N ratios are listed in Table 1 for the Ca II K, H and the combined V and R bands. The line passbands used for the S/N ratio statistics were 0.8 Å wide, centred on each line. For the Ca II lines, we adopted the same 20 Å wide V and R continuum passbands as used for Mount Wilson S index measurements. The V passband spans 3891.07 - 3911.07 Å and the R band spans 3991.07 - 4011.07 Å.

3.2 Transit light curve measurement of Hα

For Hα, we use Equation 1 with one line only, such that

$$\mathscr{F}_{H_\alpha}(t) = \frac{\overline{H_\alpha}(t)}{\overline{A}(t) + \overline{B}(t)} \quad (4)$$

The S/N ratio statistics for the Hα and the combined A and B bands (6422 − 6448 Å and 6640 − 6660 Å respectively) are tabulated in columns 8 & 9 of Table 1. Although the adopted continuum regions were chosen to ensure strong telluric H_2O lines are excluded, very weak lines of $\lesssim 1$ per cent of the normalised continuum are present in these passbands. For the Hα line itself, depending on adopted width of the band, two significant telluric lines contaminate the profile. The wavelengths of these lines are 6562.45 Å and 6563.51 Å with respective depths of ~ 2 per cent and ~ 7.5 per cent relative to the normalised continuum. We used the Line By Line Radiative Transfer Model (LBLRTM) code (Clough et al. 1992, 2005) to obtain model telluric spectra using temperature and pressure soundings from the Air Resources Laboratory[3], as outlined in §4.3 of Barnes et al. (2012). To account for any mismatches in radial velocity, spectral resolution and line strength (which depends on the model H_2O column density), the telluric spectra were then scaled to the observed spectra using the technique outlined in Appendix A of Collier Cameron et al. (2002). Dividing each spectrum by the scaled telluric model appropriate to that observation results in effective removal of the telluric lines. These spectra are then used to perform the subsequent analysis using Equation 4 above.

[3] http:ready.arl.noaa.govREADYamet.php

3.3 Transit light curve measurement of Na I D1 & D2 and Ca I 6122 Å

We also computed transit light curves for the Na I D1 & D2 lines and for Ca I 6122 Å line. As for Ca II H & K, we employed Equation 3 to calculate the Na I D1 & D2 fluxes, while for Ca I 6122 Å, Equation 4 was used.

3.4 Transit depth

The transit light curves obtained from applying Equations 3 & 4 are normalised to the OOT flux and then used to determine the transit depth. Since the IT flux difference is measured relative to the OOT flux, which is also non-zero, the measured transit depth depends on the width of the H, K and $H\alpha$ passbands. The depth, t_d, for a passband, or combined passband width of $\Delta\lambda$ is thus:

$$t_d(\Delta\lambda) = 1 - \frac{\overline{\mathscr{F}}_{IT}}{\overline{\mathscr{F}}_{OOT}} \quad (5)$$

where $\overline{\mathscr{F}}_{IT}$ and $\overline{\mathscr{F}}_{OOT}$ are the mean IT and OOT fluxes calculated in the passband of width $\Delta\lambda$ over the appropriate phases. We choose to define the equation this way so that t_d is a positive value if excess absorption is detected. For the transit light curve analysis, we define IT phases as those that lie between contact points 2 and 3 (Haswell 2010). Winn et al. (2007) measured these contact points as $\phi_3 = -\phi_2 = 0.00946$ and $\phi_4 = -\phi_1 = 0.01716$. Simultaneous modelling of both photometric and spectroscopic data has yielded $\phi_4 = 0.01696$ (Triaud et al. 2009) from which we estimate $\phi_3 = 0.00935$ by scaling the Winn et al. (2007) ϕ_3/ϕ_4 ratio. Using the parameters given by Agol et al. (2010) and the radius of Sing et al. (2011) defined in the 3700 - 4200 Å band (i.e. the band containing Ca II H & K), the analytical equations defining the total transit duration, t_T, and full transit duration, t_F (Seager & Mallén-Ornelas 2003), yield $\phi_3 = 0.00935$ and $\phi_4 = 0.01707$. We adopt these values at all wavelengths, but note that for Hα, where the radius of HD 189733b is slightly smaller (i.e. assuming the 6500 - 7000 Å band radius given by Pont et al. 2008), the contact points may be very slightly modified $\phi_3 = 0.00936$ and $\phi_4 = 0.01706$.

4 TRANSIT LIGHT CURVES

In Fig. 1, the normalised transit light curves are shown for Transits 1 - 3. The passband width, $\Delta\lambda$, was adjusted to maximise the confidence in the measured value of t_d. The procedure is described in §4.1 below and removes the transit of the opaque planet, so these curves are additional signal in the line. The contact phases for the HD 189733b transit (Winn et al. 2007), ϕ_1 - ϕ_4, are indicated by the shaded regions in Fig. 1. The light curves are all normalised to unity outside transit. With 300 sec exposures, the sampling cadence during Transit 2 shows the clearest evidence of excess absorption. However, owing to the short interval for which HD 189733b is visible, the transit is not complete. The 600 - 900 sec exposures during Transit 1 yielded the highest S/N ratios of all three transits, but at the cost of temporal resolution. Transit 1 also shows evidence for additional absorption in both light curves during transit, but the OOT levels

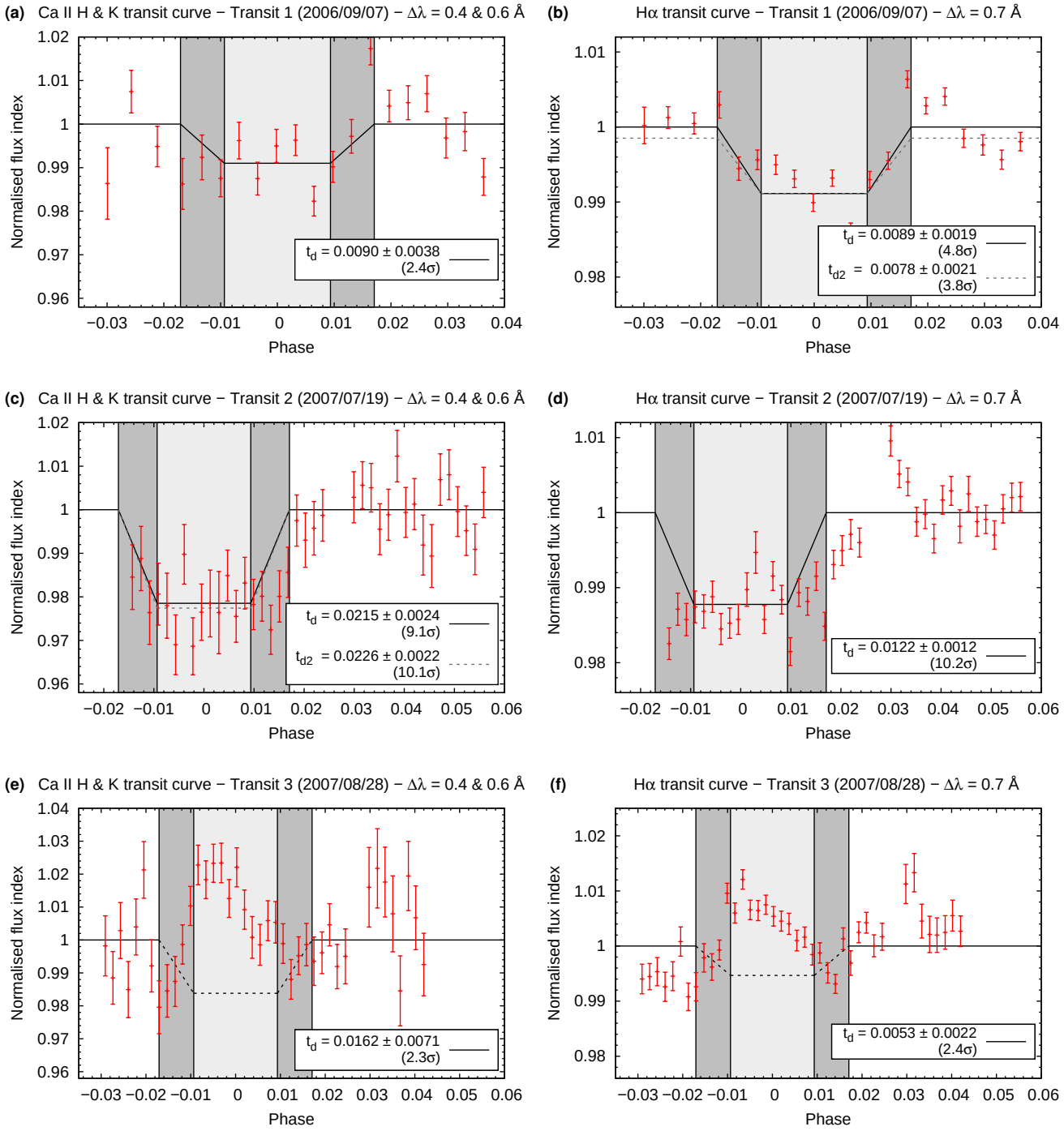
(a) Ca II H & K transit curve − Transit 1 (2006/09/07) − Δλ = 0.4 & 0.6 Å
(b) Hα transit curve − Transit 1 (2006/09/07) − Δλ = 0.7 Å
(c) Ca II H & K transit curve − Transit 2 (2007/07/19) − Δλ = 0.4 & 0.6 Å
(d) Hα transit curve − Transit 2 (2007/07/19) − Δλ = 0.7 Å
(e) Ca II H & K transit curve − Transit 3 (2007/08/28) − Δλ = 0.4 & 0.6 Å
(f) Hα transit curve − Transit 3 (2007/08/28) − Δλ = 0.7 Å
Normalised flux index
Phase
t_d = 0.0090 ± 0.0038 (2.4σ)
t_d = 0.0089 ± 0.0019 (4.8σ)
t_d2 = 0.0078 ± 0.0021 (3.8σ)
t_d = 0.0215 ± 0.0024 (9.1σ)
t_d2 = 0.0226 ± 0.0022 (10.1σ)
t_d = 0.0122 ± 0.0012 (10.2σ)
t_d = 0.0162 ± 0.0071 (2.3σ)
t_d = 0.0053 ± 0.0022 (2.4σ)

Figure 1. Differential transit fluxes for Ca II H & K and Hα with the signature of the continuum light blocked by the opaque planet removed. The panels show Transit 1 (a & b) and Transit 2 (c & d) and Transit 3 (e & f). For Ca II H & K, line core fluxes are calculated in a combined 0.4 Å (H) and 0.6 Å (K) passband (a, c & e). For Hα, line fluxes are calculated in a 0.7 Å passband. The ϕ_1 to ϕ_2 and ϕ_3 to ϕ_4 partial transit phases are shown by the darker grey shaded regions, while the full transit phases ϕ_2 to ϕ_3 are denoted by the lighter grey regions. The transit depth is determined from the mean difference between the OOT flux, where $\phi < \phi_1$ and $\phi > \phi_4$ (white regions) and the IT flux, where $\phi_2 < \phi < \phi_3$. The transit outlines are intended to guide the eye and are not transit model fits that include geometric and limb-darkening effects. The Transit 1 data have been normalised using all OOT observations (solid/black lines) and for Hα, excluding the first 2 observations after ϕ_4 (dashed/grey line), which are possibly associated with a flare. Similarly, for the Transit 2 Ca II H & K light curves (c), the transit outlines are shown by the solid/black line while the dashed/grey line shows the transit without the outlying observation at $\phi = -0.0039$. Transit 3 light curves are affected by a rise in emission, characteristic of a flare. Tentative transit depths calculated using the partial transit regions for Transit 3 are indicated and shown by dashed lines in panels e & f (see §4.3 for details).

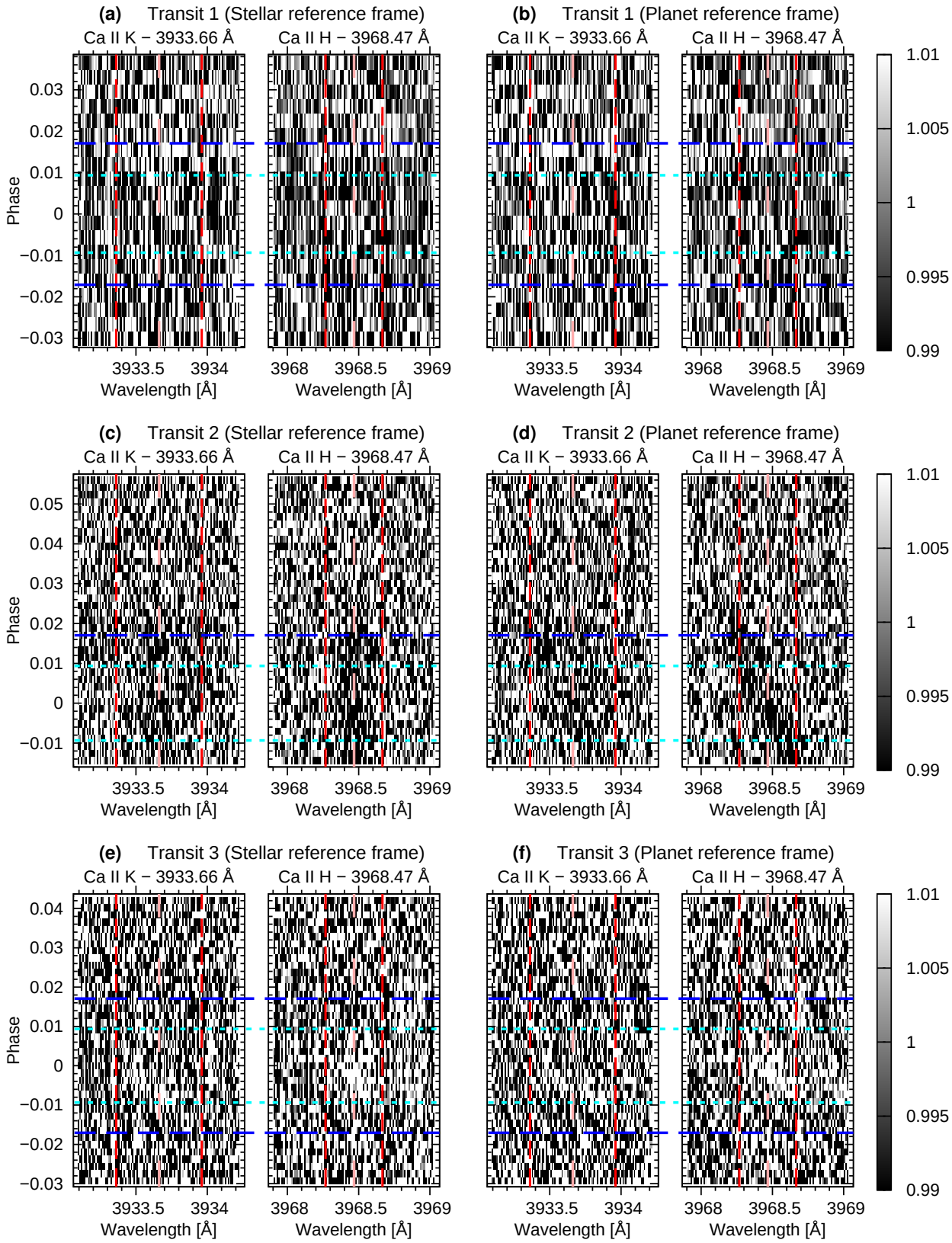

Figure 2. Normalised residual Ca II H & K time series for each transit of HD 189733b: Transit 1 (panels a & b), Transit 2 (panels c & d) and Transit 3 (panels e & f). The left hand panels (a, c & e) are the stellar reference frame time series, while the right hand panels (b, d & f) are time series shifted into the planetary reference frame. The rest wavelength of each line is indicated by a vertical, long-dashed/pink line. The vertical dashed/red lines indicate the central ±0.3 Å and ±0.2 Å ($\Delta\lambda$ = 0.6 & 0.4) regions bracketing the emission cores of Ca II K and Ca II H respectively. The first and fourth contact points of the transits, ϕ_1 and ϕ_4, are indicated by the dashed/blue lines. ϕ_2 and ϕ_3 are marked by the dotted/cyan lines.

Table 2. Transit 2 light curve depth measurements for Ca II H & K combined and for Hα. Bandwidths over which flux is measured are given on columns 1, 2, 3 & 6. The transit depths, t_d, are tabulated in columns 4, 5 & 7 and include the propagated formal uncertainties. The related significance of t_d is shown in brackets. The transit depths for Ca II H & K excluding the outlying observation at phase $\phi = -0.0039$ are listed in column 5.

Ca II H & K					Hα	
$\Delta\lambda_H$	$\Delta\lambda_K$ [Å]	$\Delta\lambda_{H+K}$	t_d	t_d (excluding $\phi = -0.0039$)	$\Delta\lambda$ [Å]	t_d
0.3	0.3	0.6	0.0265 ± 0.0031 (8.5σ)	0.0276 ± 0.0031 (9.0σ)	0.6	0.0124 ± 0.0012 (10.0σ)
0.4	0.4	0.8	0.0223 ± 0.0024 (9.4σ)	0.0231 ± 0.0023 (9.9σ)	0.7	0.0122 ± 0.0012 (10.2σ)
0.4	0.6	1.0	0.0215 ± 0.0024 (9.1σ)	0.0226 ± 0.0022 (10.1σ)	0.8	0.0111 ± 0.0011 (9.8σ)
0.6	0.6	1.2	0.0180 ± 0.0020 (8.6σ)	0.0188 ± 0.0021 (9.2σ)	1.0	0.0103 ± 0.0010 (9.9σ)
0.8	0.8	1.6	0.0161 ± 0.0022 (8.5σ)	0.0172 ± 0.0020 (7.3σ)	1.3	0.0079 ± 0.0011 (7.2σ)

are less reliably determined as there are only 9 OOT observations. Both Ca and Hα indicate flaring activity during Transit 3, with a sharp rise in flux between ϕ_1 and ϕ_2 followed by a gradual decay. The seeing during Transit 3 was also the least stable of the three sets of observations.

The normalised residual time series spectra of the Ca II H & K and Hα lines are plotted in Fig. 2 and Fig. 3 respectively (panels a, c & e). The time series in panels a, c & e were created by firstly dividing each spectrum by the mean continuum passband values defined by the denominator in Equations 3 & 4 i.e. the Ca II H & K lines were divided by $\overline{V}(t) + \overline{R}(t)$ and the Hα spectra were divided by $\overline{A}(t) + \overline{B}(t)$. From the continuum-normalised spectra, the mean OOT (as defined above in §3.4) spectrum for each region was calculated and used to normalise each spectrum in turn. This divides out any non-variable spectral features: Figs. 2 & 3 are trailed spectra showing the variations from the mean. Contact phases are indicated by the horizontal dashed and dotted lines (see Fig. 2 caption for details). For Transits 1 & 2, the Hα time series in Fig. 3 (a, c & e) clearly show evidence for additional absorption during the IT period. The excess absorption in Ca II H & K is only clearly seen during Transit 2 in Fig. 2. Both Ca II H & K, and Hα show the emission attributable to stellar activity during Transit 3, which is revealed in the transit light curves in Fig. 1, and which precludes measurement of any excess absorption. We attribute this to a flaring event that takes place near the start of Transit 3.

In §4.1 below, we initially focus our analysis on the 39 Transit 2 observations, which show the strongest evidence of excess absorption in the Ca II H & K and Hα lines. The 20 observations from Transit 1 are then considered in a similar manner in §4.2 with brief comments on the Transit 3 observations in §4.3.

4.1 Transit 2 light curves

Fig. 4 (a) shows the core regions of Ca II K, H and Hα for IT and OOT spectra. The lines have been corrected to the rest wavelength in air, denoted by the long-dashed vertical lines (the velocity corrections ranged from -6.8 to -6.5 km s^{-1} during the observations). The telluric lines present in the Hα line, which vary in strength with airmass, have been corrected for using the method outlined in §3.2. For Transit 2, 11 exposures fall within the ϕ_2 - ϕ_3 IT range, while 19 exposures were taken at OOT phases (i.e. taken at phases $> \phi_4$). Looking at the centres of the line profiles, it is clear that there is more absorption in all three lines during IT compared with OOT phases. The residuals are plotted in Fig. 4 (b) and show the mean excess absorption in each case, with the wavelength scale replaced by the equivalent velocity in the rest frame of each line. The width of the additional IT absorption appears to be greater in the emission core of Ca II K compared with Ca II H. Ca II K is the stronger line in stellar spectra because while the Ca II H and Ca II K arise from a transition with the same lower state, the upper states differ. The different degeneracies of the upper two levels results in an enhanced source function of K over H in the upper chromosphere of the star (Rauscher & Marcy 2006). Measurement of transit depths must take account of the different widths of any excess absorption by adapting passband widths for flux measurement.

The transit excess due to Na in the atmosphere of HD 209458b was measured by Charbonneau et al. (2002), who considered the flux in passbands of three different widths. Subsequent analyses by Redfield et al. (2008), Snellen et al. (2008) and more recently by Wyttenbach et al. (2015) using the spectra discussed herein, have also investigated the significance of the detection with different passband widths. The method of flux measurement outlined in §3 does not account for the radial velocity of the planet during transit. As noted by Wyttenbach et al. (2015), the radial velocity of HD 189733b spans −15.9 to +15.9 km s^{-1} in the $\phi_1 - \phi_4$ interval. Between ϕ_2 and ϕ_3, the range of velocities is −8.47 to +8.47 km s^{-1}. We consider only phases $\phi_2 < \phi < \phi_3$ when measuring the transit depth. At air wavelengths of $\lambda = 3933.66$ Å, 3968.47 Å and 6562.79 Å for Ca II H, K and Hα (Kramida et al. 2015), absorption from HD 189733b in the ϕ_2 - ϕ_3 range will lie within ±0.113 Å ±0.114 Å and ±0.188 Å respectively. Hence minimum filter widths for calculating the line fluxes of $\Delta\lambda = 0.226$ Å, 0.228 Å and 0.377 Å should be used to ensure all absorption co-moving with the planet is included in the IT observation phases.

4.1.1 Ca II H & K

For the Ca II H & K lines, we measured the transit depth in passbands of $\Delta\lambda$ = 0.3, 0.4, 0.6 & 0.8 Å for each line (i.e. combined passband widths of $\Delta\lambda$ = 0.6, 0.8, 1.2 & 1.6 Å).

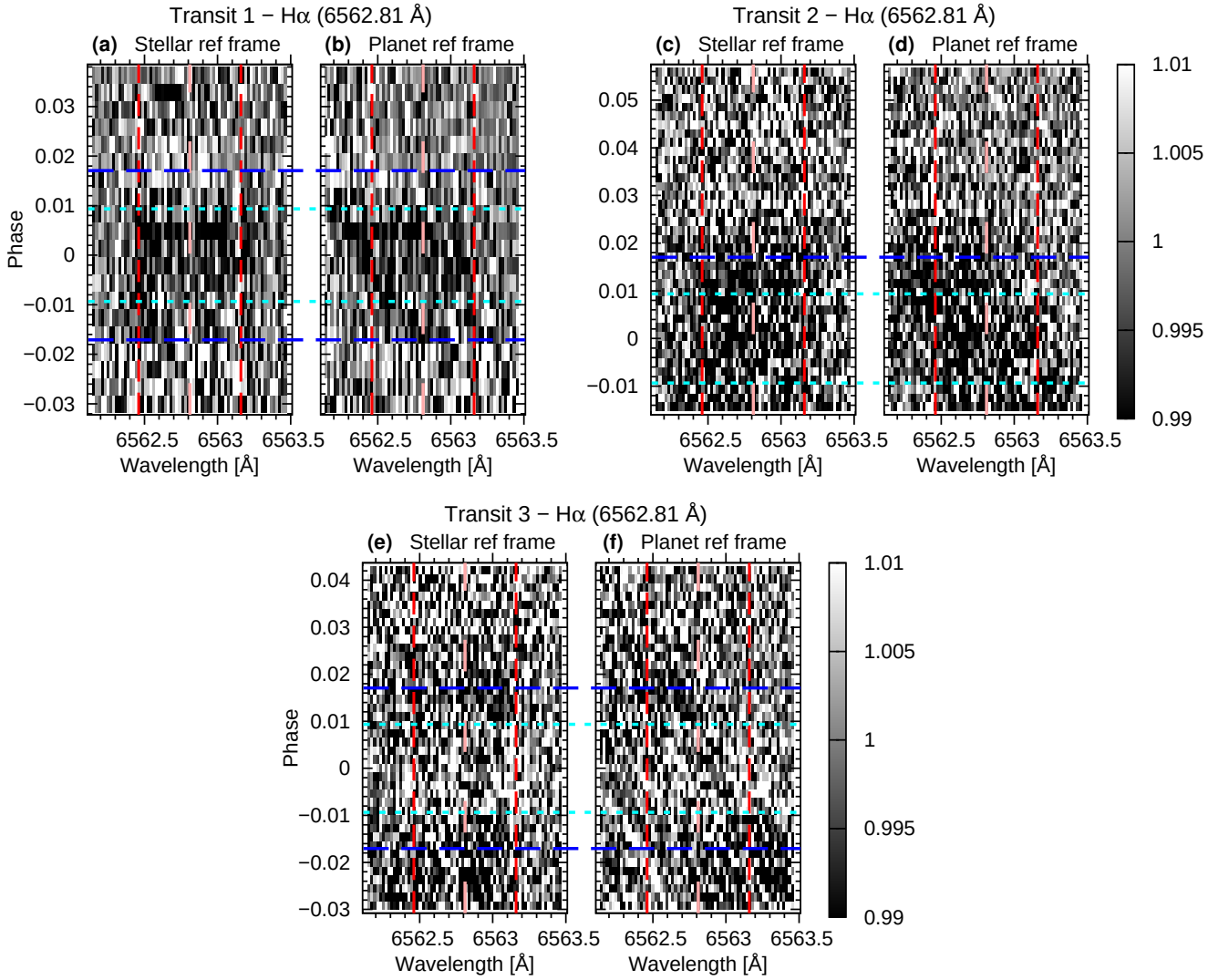

Figure 3. As for Fig. 2 with the Hα (6562.81 Å) line. The vertical dashed/red lines indicate the central ±0.35 Å ($\Delta\lambda$ = 0.7 Å) for which the excess absorption during transit is optimised.

These passband limits are marked by the short-dashed lines in Fig. 4. Since the absorption feature in the Ca II K line is broader than the Ca II H line, we also tried a combined passband of 0.4 Å for H and 0.6 Å for K, giving a 1.0 Å effective total passband. The results are listed in Table 2. The individual passband widths for Ca II H and K are listed in columns 1 & 2, along with the combined passband, which is simply the sum of columns 1 & 2. Using equal passbands and all observations to measure t_d, the transit depth is detected with greatest significance for the combined 2×0.4 Å passband, with $t_d = 0.223 \pm 0.0024$. We also investigated removal of the outlying point at $\phi = -0.0039$, which may simply be a statistical outlier. With this point removed, the Ca II H & K transit depth, t_d, is detected with greatest significance for the combined passband of 1.0 Å, which utilises the Ca II H and Ca II K widths of 0.4 Å and 0.6 Å respectively. Fig. 4 (a) shows that these respective widths correspond to the widths of the core emission reversals as defined by the points either side of the centre of the line at which the second derivative of the flux with respect to wavelength is maximised. With a combined 1.0 Å passband, we detect additional absorption due to Ca II with $t_d = 0.0226 \pm 0.0022$ (2.26 ± 0.22 per cent) at a significance of 10.1σ.

4.1.2 Hα

For Hα, the use of single passbands in the range $\Delta\lambda = 0.6 - 1.3$ Å were investigated. Table 2 shows that excess absorption due to Hα is most significantly detected in a 0.7 Å passband, with $t_d = 0.0122 \pm 0.0012$ (1.22 ± 0.12 per cent) and a significance of 10.2σ. Despite using only a single line, the same significance compared with the excess absorption in Ca II H & K can be attributed to the higher S/N ratios at Hα (see Table 1).

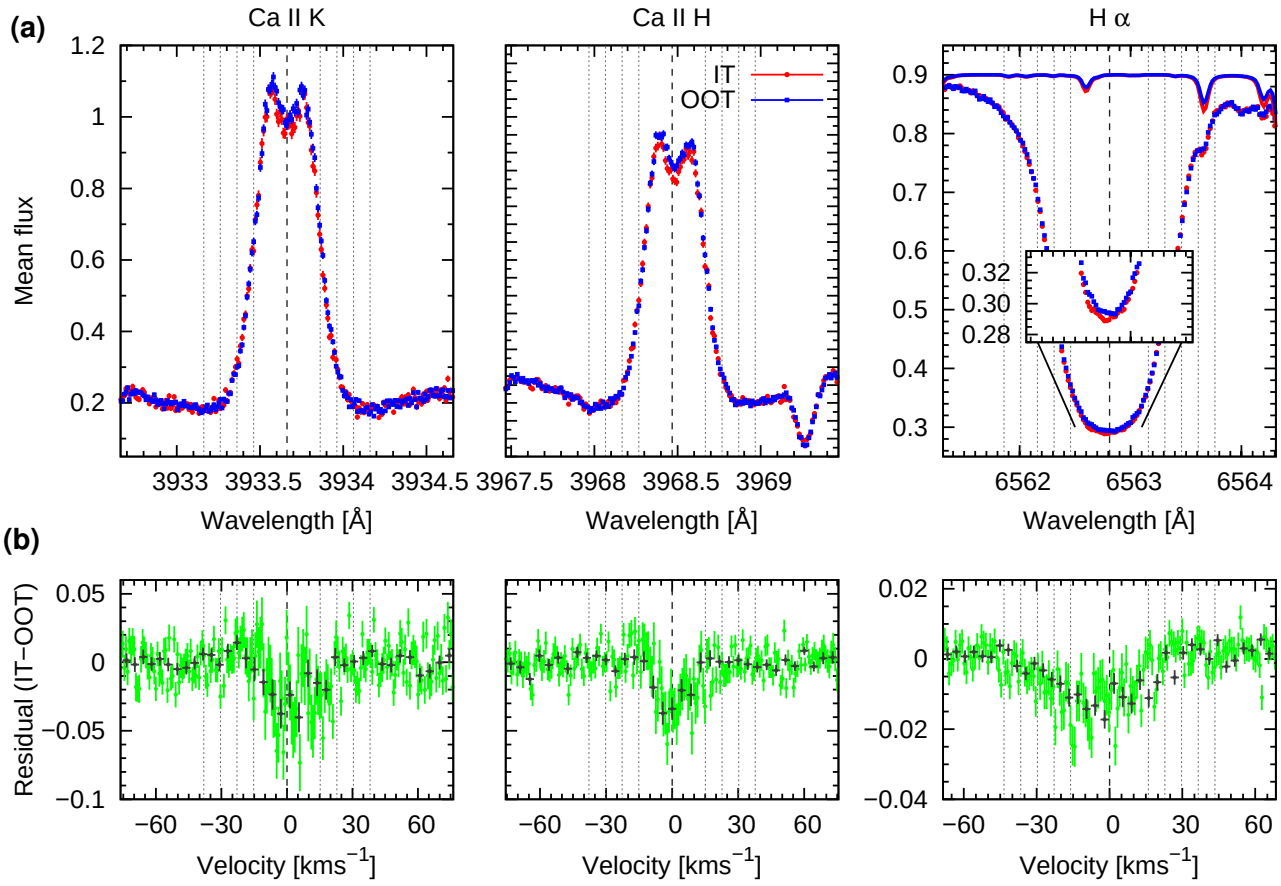

Figure 4. (a) Transit 2 averaged Ca II H & K and Hα lines in transit (IT, red circles) and out of transit (OOT, blue squares). All points are plotted with uncertainties. The out of transit profiles were normalised to the mean continuum regions, as described in §4.1 before averaging. The inset for Hα is plotted with the same x-scale as the main axis, but with an expanded y-axis to enable the IT/OOT flux difference to be seen. The vertical dashed lines indicate the rest wavelength of each spectral line. For the Ca II H & K plots, the dotted vertical lines show the $\Delta\lambda = 0.3, 0.4, 0.6$ & 0.8 widths in Table 2 over which the line fluxes were calculated. Similarly for Hα, the $\Delta\lambda = 0.6, 0.7, 0.8, 1.0$ & 1.3 regions are indicated. (b) Residual IT - OOT profiles in the reference frame of HD 189733. Unbinned points are shown in green, while the black points are averaged into 0.05 Å and 0.075 Å bins for Ca II and Hα respectively. Bin widths are indicated on the residual plots by the horizontal bars.

4.2 Transit 1 light curves

We used the same optimised passbands as for Transit 2 to obtain Transit 1 light curves, which also show excess absorption, albeit with lower significance (Fig. 1, a & b). We find $t_d = 0.0090 \pm 0.0038$ (0.90 ± 0.38 per cent; significance 2.4σ) for Ca II H & K and $t_d = 0.0089 \pm 0.0019$ (0.89 ± 0.19 per cent; significance 4.8σ) for Hα. The transit depths for Transit 1 are highly sensitive to the few OOT observations, which show considerable scatter. A possible cause may be small flaring events. Observations of Proxima Centauri (M6V) have shown that following a flare event, elevated Ca II H & K fluxes decay more rapidly than Hα (Fuhrmeister et al. 2011). If the outlying point in the Ca II H & K light curve at $\phi = 0.0164$ (between ϕ_3 and ϕ_4) is due to a small flare, it is possible that phases ($\phi = 0.0164$, 0.0197 & 0.02304) are all affected in the Hα light curve for Transit 1. Obviously, more data points would have be en desirable to verify this with greater statistical confidence. Nevertheless, removing the two OOT points at $\phi = 0.0197$ & 0.02304 from the Hα time series, which are used to normalise the light curve, we find $t_d = 0.0078 \pm 0.0021$ (3.8σ). In §4.4 we perform a more robust empirical Monte Carlo simulation to better assess the significance of Transit 1 and Transit 2 estimates of t_d (Fig. 5).

4.3 Transit 3 light curves

For Transit 3, the light curves do not permit accurate measurement of any excess absorption in Ca II H & K and Hα owing to the rise in emission in the cores of both Ca II H & K and Hα at the start of the transit. The elevated flux lasts for most of the transit, but appears to return to a level below that of the mean OOT phases somewhere in the $\phi_3 - \phi_4$ interval. The transit depths shown in the bottom panels of Fig. 1 have been measured by taking the mean of two flux measurements, namely the minimum light curve flux in the $\phi_1 - \phi_2$ region and the $\phi_3 - \phi_4$ region. These measurements can be taken as lower limits to t_d for Transit 3. However it is possible that variable flaring activity is present throughout the transit, which may result in an estimate of t_d that is significantly underestimated.

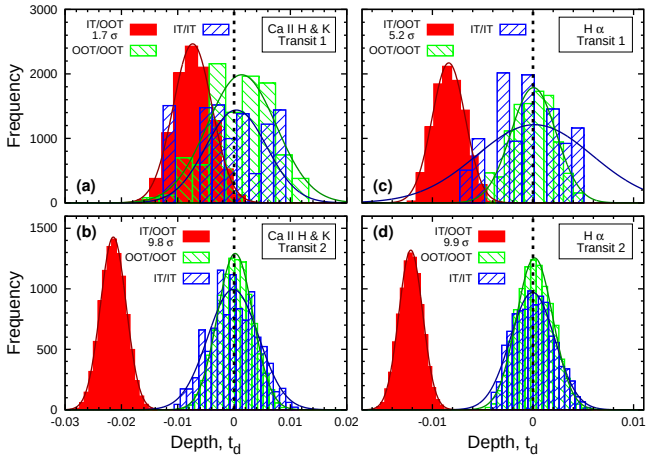

Figure 5. Empirical Monte Carlo analysis of the Transit 1 & 2 light curves for Ca II H & K and Hα.

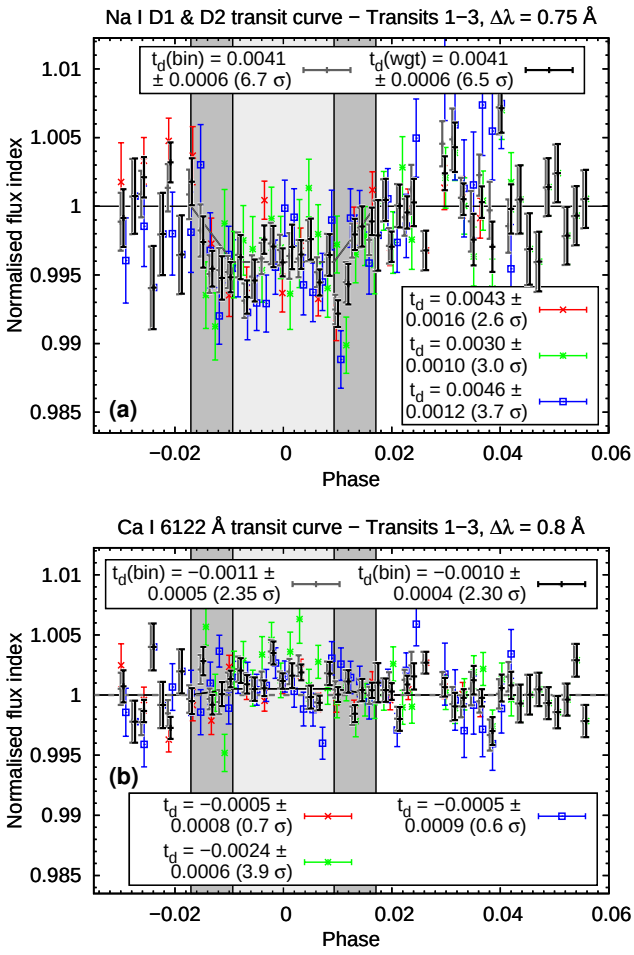
Na I D1 & D2 transit curve − Transits 1−3, Δλ = 0.75 Å
t_d(bin) = 0.0041 ± 0.0006 (6.7 σ)
t_d(wgt) = 0.0041 ± 0.0006 (6.5 σ)
t_d = 0.0043 ± 0.0016 (2.6 σ)
t_d = 0.0030 ± 0.0010 (3.0 σ)
t_d = 0.0046 ± 0.0012 (3.7 σ)
(a)
Normalised flux index
Phase
Ca I 6122 Å transit curve − Transits 1−3, Δλ = 0.8 Å
t_d(bin) = −0.0011 ± 0.0005 (2.35 σ)
t_d(bin) = −0.0010 ± 0.0004 (2.30 σ)
t_d = −0.0005 ± 0.0008 (0.7 σ)
t_d = −0.0005 ± 0.0009 (0.6 σ)
t_d = −0.0024 ± 0.0006 (3.9 σ)
(b)
Normalised flux index
Phase

Figure 6. (a) Transit light curves for the combined Na 1 D1 (5995.924 Å) and D2 (5889.951 Å) lines. The mean light curves are shown in grey (unbinned) and black ($\Delta\phi = 0.002$ bins). (b) Transit light curve for the Ca I 6122 Å line, plotted with the same axes as panel (a).

4.4 Significance of t_d from empirical Monte Carlo

To better assess the significance of the excess absorption during transit, we have performed an empirical Monte Carlo simulation in a similar manner to that initiated by Redfield et al. (2008), and later adopted by Astudillo-Defru & Rojo (2013), Cauley et al. (2015) and Wyttenbach et al. (2015). The key benefit of the simulations is that they enable the inclusion of atmospheric, instrumental and astrophysical uncertainties that are not fully characterised by the photon noise. The procedure is more critical in establishing the significance of Transit 1 than Transit 2, where the excess absorption at transit phases is more clearly defined. Nevertheless, this procedure enables the propagated formal uncertainties that we have used so far (see Table 2) to be assessed robustly. We did not attempt to assess the Transit 3 data in this way.

Three scenarios are simulated, using (1) only OOT observations, (2) only IT observations and (3) IT and OOT observations. For the purposes of the simulation, we assumed IT observations were those observed in the range $\phi_2 \leq \phi \leq \phi_3$ from which we measured t_d above. Similarly, the OOT observations are defined as phases where $\phi < \phi_1$ or $\phi > \phi_4$. For scenarios (1) and (2), half the observations were selected at random (without replacement) and then subdivided into two data sets in the same ratio as the actual observed IT and OOT observations. The transit depth, t_d, was calculated from the mean of the two simulated data subsets. The process was repeated 10,000 times, picking a random number of observations each time. The same procedure was adopted for scenario (3), but the two data subsets were drawn from the IT observations and the OOT observations separately. We expect that scenarios (1) and (2) should produce distributions that are consistent with $t_d = 0$, while scenario (3) should yield the same, or similar values of t_d to the measurements made on the full data sets.

Fig. 5 shows the resulting distributions of t_d for the combined Ca II H & K and Hα light curves for Transit 1 and Transit 2. Redfield et al. (2008) and Wyttenbach et al. (2015) used the distribution width from scenario (1) using OOT observations only, as these phases are free of any transit effects. Since fewer data points are used compared with the measurement of t_d from the full data set, the width of the scenario (2) distributions must be corrected by dividing the determined standard deviations of the simulated t_d values by the square root of the ratio of the total IT+OOT observations to the OOT observations. For Ca II H & K, we find respective Transit 1 and Transit 2 depths of $t_d = 0.0074 \pm 0.0044$ and $t_d = 0.0214 \pm 0.0022$ (i.e. 1.7σ and 9.8σ detections). For Hα, we similarly find $t_d = 0.0084 \pm 0.0016$ and $t_d = 0.0121 \pm 0.0012$ (i.e. 5.2σ and 9.9σ detections). The empirical Monte Carlo transit depths and significance values are also shown in Fig. 5 and are in good agreement with the measurements of t_d in Table 2 (columns 4,5 & 7) that use the propagated formal errors. The significance of the detections in each case are slightly reduced owing to excess variability above the photon noise level.

4.5 Na I D1 & D2 and Ca I 6122 Å

4.5.1 Na I D1 & D2 transit light curves

Since the depth of the excess absorption during transit appears to be variable from one epoch to another, we re-

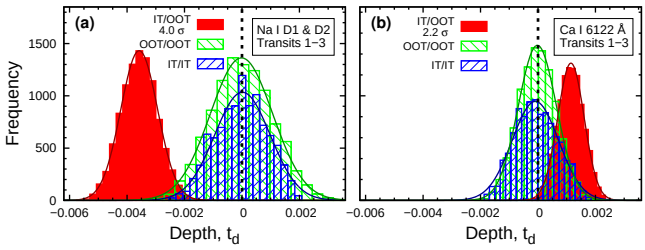

Figure 7. Empirical Monte Carlo analysis of the transit light curves for Na I D1 & D2 and Ca I 6122 Å lines.

analysed the Na I D1 & D2 lines at 5889.95 Å and 5895.92 Å for Transits 1 - 3 individually. As these lines have previously been studied in detail by other authors, and particularly, extensively and thoroughly by Wyttenbach et al. (2015) using the same data set as we are using, we adopted similar parameters throughout this paper. Here, we repeat the analysis, but also present the light curves for individual transits, as above for Ca II H & K and Hα. For consistency with Wyttenbach et al. (2015), we used 0.75 Å passbands to derive the light curves, and have optimally combined the flux in both the D1 and D2 line cores in the same manner as for Ca II H & K.

Fig. 6 (a) shows the light curve for each transit and combined light curves using the data from all three transits, binned into $\Delta\phi = 0.001$ intervals. The un-weighted, binned, light curve is shown in grey, while the weighted, binned, light curve is shown in black. The weighted light curve using the three transits, is more appropriately adopted since it takes into account the measurement uncertainties in the individual transits. We find $t_d = 0.0041 \pm 0.0006$ (6.5σ) for the weighted mean light curve for Na I D1 & D2.

Unlike Ca II H & K and Hα, Transit 2 shows the shallowest depth in Na I D1 & D2. This result is not significant since all three transits agree within the uncertainties (see Fig. 6). We note however that Wyttenbach et al. (2015) report an even shallower Transit 2. Our measured t_d using all three transits is marginally larger than the value reported by Wyttenbach et al. (2015) who find $t_d = 0.00325 \pm 0.00033$ when averaging Transits 1 - 3. Both results however agree within the 1σ measurement uncertainties. Fig. 7 (a) shows the empirical Monte Carlo analysis applied to the weighted and binned Na I D1 & D2 light curve. We find $t_d = 0.0036 \pm 0.0009$ (4.0σ), bringing our estimate into closer agreement with that of Wyttenbach et al. (2015).

4.5.2 Control light curve using Ca I 6122 Å

Ca I 6122 Å, a strong absorption line that does not contain a chromospheric component, was used by Redfield et al. (2008) as a control line. Cauley et al. (2015) similarly used three other Ca I transitions as control lines. No transmission signature was found in these lines, in accordance with the findings of Lodders (1999) that Ca I is only present in very low abundance in planetary atmospheres. We plot the light curve during transit of Ca I 6122 Å in Fig. 6 (b), which shows that an obvious transit signature with significant absorption, as seen in the other lines, is not discernible.

Low level emission in Ca I 6122 Å is instead seen with marginal 2.3σ significance, with $t_d = -0.0010 \pm 0.0004$ (the negative sign represents relative emission during transit). The empirical Monte Carlo simulation in Fig. 7 (b) similarly indicates $t_d = -0.0011 \pm 0.0005$ (2.2σ). This closer agreement between formal uncertainties and Monte Carlo estimates is likely due to the line being situated close to the centre of the échelle order and the fact that it is a weaker line with more flux in the core. The S/N ratios of the line cores of Ca I 6122 Å for Transits 1 - 3 are 109.0, 73.0 and 64.5 respectively, while for Na I D1 & D2, we find 65.8 & 67.0, 43.5 & 45.4 and 39.0 & 40.1 respectively (c.f. also the S/N ratios for Ca II H & K and Hα in Table 1).

The individual transits of Ca I 6122 Å in Fig. 6 (b) show marginally greater emission during Transit 2, in agreement with the lower significance Transit 2 measurement for Na I D1 & D2. This finding may indicate that both lines are showing the signature of a starspot or starspot group during Transit 2. The relative emission during transit may result from a combination of factors (see §6). The Ca I 6122 Å light curve demonstrates that not all lines exhibit excess absorption during transit.

4.6 Airmass effects

We have considered the possibility that the observed excess absorption arises from incorrect normalisation or airmass effects at the time of observation. For the Transit 2 light curves presented in Fig. 1, we have calculated Pearson's correlation coefficient to test for a correlation of the transit light curve fluxes with airmass, X, altitude above the horizon, A (where $X = sec(A)$ for $A > 20°$), S/N ratio and seeing. We find respective correlation coefficients of $r = -0.63$, 0.70, 0.55 and 0.32 for Ca II H & K, while for Hα, we find $r = -0.75$, 0.80, 0.48 and 0.39. The correlations with S/N ratio and seeing are moderate to weak, whereas moderate to high (anti-)correlations are found with airmass and altitude. To assess the significance of this finding, we calculated the correlation between a model transit signature and the variation in airmass and altitude at the observation phases on Transit 2. We used the EXOFAST routine (Eastman et al. 2013) to create a model transit using the system parameters summarised in Table 1 of (Wyttenbach et al. 2015), but adopted U-band limb-darkening coefficients (Claret 2000) and the 3700 - 4200 Å radius measured by Sing et al. (2011). For the Ca II H & K curve, the correlation between the simulated transit fit and airmass yields $r = -0.71$, while the correlation between the transit fit and altitude yields $r = 0.79$. The change in airmass and altitude with observation times thus show a similar strong correlation with an appropriate model transit light curve. A strong correlation between the observed light curves and airmass is thus not sufficient to rule out real transit effects. Moreover, given that Na I D1 & D2 and Ca I 6122 Å do not show significant variability in depth during the three transits, we are confident that the time-variable light curves obtained for Ca II H & K and Hα are the result of activity variability on HD 189733 rather than airmass effects. Since there are also no telluric lines at the Ca II H & K core wavelengths, we are not aware of any airmass effects that could give rise to the variable absorption signal seen in the line cores in Fig. 4.

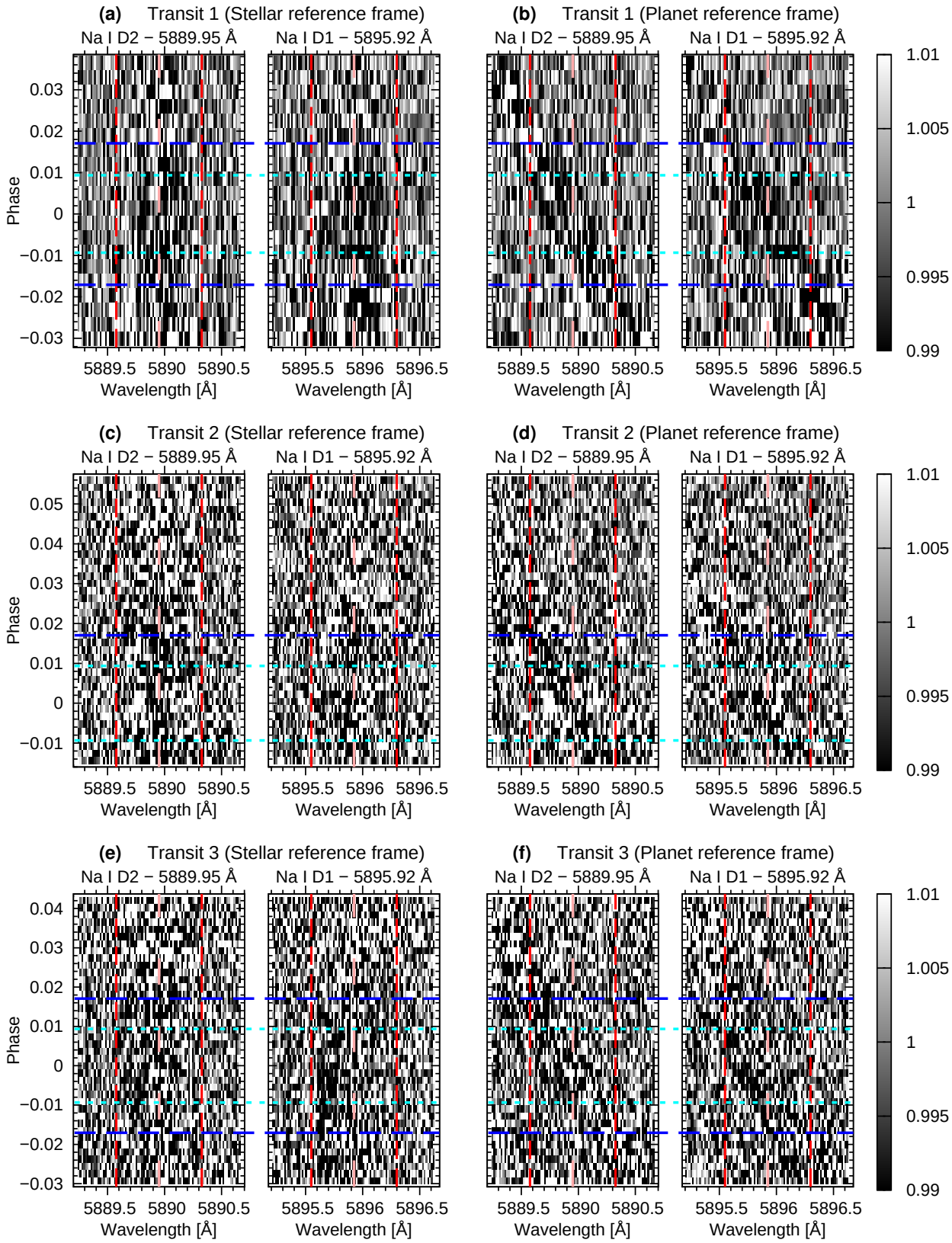

Figure 8. As for Fig. 2 with the Na I D1 & D2 (5889.951 Åand 3895.924 Å) lines. The vertical dashed/red lines indicate the central ±0.375 Å ($\Delta\lambda$ = 0.75 Å) employed in other studies.

5 TIME SERIES AND TRANSMISSION SPECTRA

The residual time series spectra in Figs. 2, 3 & 8 (a, c & e) are plotted in the stellar reference frame. Below, we investigate the time series residual spectra in further detail and use them to obtain averaged residual transit profiles.

5.1 Time series spectra in the planet reference frame

During transit, any stellar light absorbed in the atmosphere of the planet will be shifted by the instantaneous radial velocity of the planet relative to the star at the time of observation. In other words, the planetary absorption during transit should first appear at -15.9 km s^{-1} and at the end of transit will be shifted by +15.9 km s^{-1}.

We have also included a correction for the stellar rotation of HD 189733. With $v \sin i = 3.1 \pm 0.03$ km s^{-1} (Collier Cameron et al. 2010), the impact parameter of the transit (Agol et al. 2010) means that transmitted light is additionally shifted in the range ± 1.6 km s^{-1} during the transit. The picture is also modified to a smaller degree by the Rossiter-MacLaughlin effect and putative zonal winds, as inferred by Louden & Wheatley (2015) using the Transit 3 observations of this date set. We have not included Rossiter-MacLaughlin velocity corrections here as they are negligible at $\sim$30 ms^{-1} (Winn et al. 2006) compared with the other corrections. We follow the procedure adopted by Wyttenbach et al. (2015), with the additional stellar rotation correction, to optimise the signal from the planet and avoid smearing due to its phase-dependent radial velocity. The instantaneous radial velocities were calculated from the ephemeris in Agol et al. (2010) using an orbital inclination of $i = 85.7°$.

5.1.1 *Ca II H & K and Hα planet reference frame residual time series*

Figs. 2 & 3 (panels b, d & f) show the residual time series spectra in the planetary reference frame. For Ca II H & K, as with panels a, c & e (in the stellar reference frame), only the Transit 2 observations enable the absorption to be discerned by eye. For Hα the excess absorption is more readily apparent during Transits 1 & 2 in Fig. 3, with a hint of some redshifted excess absorption during Transit 3 (both panels e & f) between ϕ_1 and ϕ_4.

The most striking and unexpected feature of our analysis in this paper is the apparent red-to-blue trend of the excess absorption with phase. This appears when we shift to the reference frame moving with the planet. We expect absorption in the planet's atmosphere to be at rest in the planet's reference frame. This is particularly clear during Transit 2 in the Ca II H line and appears as a dark diagonal stripe during the transit. This is unexpected under the assumption that the excess absorption arises in the atmosphere of the planet, we would expect improved alignment of the absorption in the planet reference frame. It is clear however that panel c of Fig. 2, appears to show no such gradient in the stellar reference frame. A red-to-blue trend with advancing phase is also evident in the planet reference frame time series panels for Hα in Fig 3 (b, d, and possibly f despite the flaring event). Clearly this is a very important observation since it suggests that the excess absorption might arise in the stellar reference frame rather than the planetary reference frame.

5.1.2 *Na I D1 & D2 residual time series*

We plot time series spectra for the Na I D1 & D2 lines for each transit in Fig. 8 in both the stellar (panels a, c & e) and planet (panels b, d & f) reference frames. As with Hα, we have corrected for the effects of telluric lines. The stellar reference frame time series clearly show excess absorption during Transits 1 - 3. Since the significance of the excess absorption is smaller than for Ca II H & K and Hα (§4.1), the much lower S/N ratio in the line core regions is more evident, at both IT and OOT phases. The Na I D1 & D2 lines are clearly also less sensitive to activity variability in the chromosphere as the Transit 3 light curve still shows excess IT absorption unlike Ca II H & K and Hα. In the planet reference frame (Fig. 8, panels b, d & f), we see that the excess absorption shows a red-to-blue shift with phase for all three transits, again suggesting that the excess absorption may be stellar in origin.

The time series spectra in both the stellar and planet reference frames (Fig. 8, panels a, c & e) appear to show evidence that the excess absorption is sometimes redshifted (i.e. during Transit 1) and sometimes blueshifted (Transit 3) from the rest wavelength. For both Hα and Na I D1 & D2, the telluric line contributions are removed from the time series spectra to levels consistent with the noise before calculating the residual timeseries, as outlined in §3.2. A visual inspection of the telluric line strengths and positions, which shift against the stellar lines from one epoch to another, indicates that they are not responsible for the shift in position of the excess absorption.

5.2 Mean residual transit profiles

Average residual IT spectra were created for observations between contact phases ϕ_1 and ϕ_4. The first ground-based report of excess absorption in Na I D1 & D2 by Redfield et al. (2008) obtained spectra by subtracting a master OOT spectrum from the IT spectra individually before co-adding the IT residuals to obtain a mean IT residual spectrum with optimal S/N ratio. Any resulting excess absorption at the wavelengths of the atomic species being studied has been interpreted as a signature of the planet, without assessing the time-dependent velocity behaviour of the absorption. In contrast, and in light of our analysis in §5.1, we have created transmission profiles for Ca II H & K, Na I D1 & D2 and Hα in both the stellar reference frame and the planet reference frame.

Fig. 9 shows transmission profiles for each line for Transits 1 - 3 in both the stellar and planet reference frames, as indicated. The plots maintain the same scales for a given line in both reference frames, and for each transit. A Gaussian profile has been fitted to each spectrum to obtain an estimate of the velocity offset of the feature, v (km s^{-1}), relative to the rest wavelength of each line, the Gaussian width, w (in km s^{-1}), and the normalised depth, d. The three parameters, along with formal uncertainties, are indicated in each

panel. A positive value of d indicates absorption. Since Transit 3 is affected by excess chromospheric activity, and we do not detect excess absorption in Ca II H & K, it is not surprising that meaningless fits are obtained. As expected from our findings in §4, all lines show the strongest absorption during Transit 2.

5.2.1 *Transmission profile differences in the stellar and planet reference frame*

Fig. 10 (a) displays the measured v, d and w, for each line in the stellar (open symbols) and planet (closed symbols) reference frames for each line. In Fig. 10 (b), the relative difference significance of the planet minus the stellar reference frame measurement (e.g. for the profile width, w, $\sigma(w_p - w_s) = (w_p - w_s)/\sqrt{\Delta w_p^2 - \Delta w_s^2}$) is plotted for each parameter. Transit 1 (red sqaures) is only marginally detected in most lines. Consistent with this, the difference between the transit line profile in the two frames of reference is not significant: for Transit 1, only Na I D2 shows $\sigma(w_p - w_s)$ and $\sigma(d_p - d_s) > 1$, while Na I D1 shows respective significances of ~ 1. For the Ca II H & K and Hα lines, any differences are very low confidence, with $|\sigma(w_p - w_s)| < 1$ and $|\sigma(d_p - d_s)| < 1$. In other words, marginally narrower and deeper profiles are seen *in the stellar reference frame* during Transit 1 only for the less chromospherically sensitive Na I D1 & D2 lines.

In Fig. 9, the Transit 2 plots (columns 3 and 4) reveal that *all profiles are deeper and narrower in the stellar reference frame*, although the significance is still lower in Ca II K and Hα. For Ca II H, Na I D1 & D2, $1 \lesssim \sigma(w_p - w_s) \lesssim 3$. For Transit 3, Na I D1 & D2 show similar results to Transit 1 on average. While the Ca II H & K lines are strongly affected by the chromospheric activity transient, the Hα absorption profile remains marginally sharper in the stellar reference frame, but with low significance, as at all other epochs, likely due to the fact that the feature is broader than the other lines. Finally, the significance of the difference between the reference frames of the velocity offsets from the rest wavelengths, $\sigma(v_p - v_s)$, is potentially less important, but we include it for completeness.

6 DISCUSSION

Excess absorption is seen in some or all of the Ca II H & K, Hα and Na I D1 & D2 lines during all three transits. The sensitivity of the Ca II H & K lines to chromospheric transients are a notable obstacle to detecting transit signatures in these lines, as evidenced by the Transit 3 observations. This problem was encountered by Czesla et al. (2015) in their study of the centre-to-limb brightening of Ca II H & K and Na I D1 & D2 with high S/N ratio UVES observations.

Despite extending and confirming previous results, our study reveals some surprises. Firstly, from space-based observations, it is not clear that Ca II should show strong excess absorption in the atmosphere of a close orbiting giant exoplanet such as HD 189733b. Observations by Pont et al. (2008) and Sing et al. (2011) with the Hubble Space Telescope (HST) did not initially detect either Ca or Na. Pont et al. (2013) were able to identify Na absorption by adopting a narrower passband, but at a lower level than predicted. The detection of relatively weak absorption only in narrow regions centred on the Na lines added weight to the earlier suggestion (Lecavelier Des Etangs et al. 2008) that a Rayleigh scattering haze is responsible for obscuring all but strong, sharp, line cores. While Sing et al. (2011) and Pont et al. (2013) demonstrate that a haze is detected at short wavelengths, masking planetary spectral features, the cloud-free model transmission spectra of Fortney et al. (2010) *do* lead us to expect absorption from the Ca II H & K lines (e.g. see also Figs. 10 & 11 in Pont et al. 2013). With the increasing importance of Rayleigh scattering at shorter wavelengths and the lower S/N ratios, it is not surprising that detection at Ca II H & K was not made by Sing et al. (2011) or Pont et al. (2013).

The ground-based observations of Redfield et al. (2008) and Wyttenbach et al. (2015) have used high resolution spectroscopy and similarly show excess absorption in the cores of Na during transit of HD 189733b. Other studies have also claimed excess absorption in the Hydrogen Balmer lines of HD 189733b (Cauley et al. 2015). In this paper, we also find variable absorption in broad agreement with the Na I D1 & D2 results in Wyttenbach et al. (2015), but further, we find that absorption strength is variable from transit to transit in all the lines studied, though the significance in Na I D1 & D2 is uncertain. This suggests either that the structure of the upper layers of the planetary atmosphere may be variable, or that stellar variability to some degree may instead be responsible for the excess absorption.

In addition to the variable nature of the transits, we find that the excess absorption is narrowest and deepest when the time resolved spectra are co-added in the stellar reference frame. This is clear and obvious in the ten panels of Fig. 9 showing results from Transit 2. Although the significance of the differences between excess absorption profile widths and depths, $\sigma(w_p - w_s)$ and $\sigma(d_p - d_s)$ (§5.2.1), are relatively low for some lines (i.e. Ca II K and Hα), the Na I D1 & D2 lines taken together consistently appear sharper in the stellar reference frame. This is probably due to the narrow Na I D1 & D2 line cores. Similarly, the Ca II H profile appears significantly sharper in the stellar reference than the planetary reference frame (as quantified by $\sigma(w_p - w_s)$ and $\sigma(d_p - d_s)$) during Transit 2, whereas Ca II K does not because it is intrinsically broader as explained in §4.1.

For the sharpest features in Figs. 2, 3 & 8, we have further verified that the apparent red-to-blue shift of the excess absorption in the planet reference frame is real. We summed residual spectra in the planet reference frame between ϕ_1 and ϕ_2 (Profile 1) and also between ϕ_3 and ϕ_4 (Profile 2). Within the measurement uncertainties, the difference between the measured velocities of Profile 1 and Profile 2 is identical to the phase dependent shift applied to translate the spectra into the planet reference frame. This further confirms our suspicion that the excess absorption, or at least the more significant part of it, is located in the stellar reference frame.

6.1 The reliability of transmission spectra in chromospherically sensitive lines

Ground-based transmission spectroscopy using high-resolution spectrometers must normalise the flux to account for the non-constant flux levels from seeing and instru-

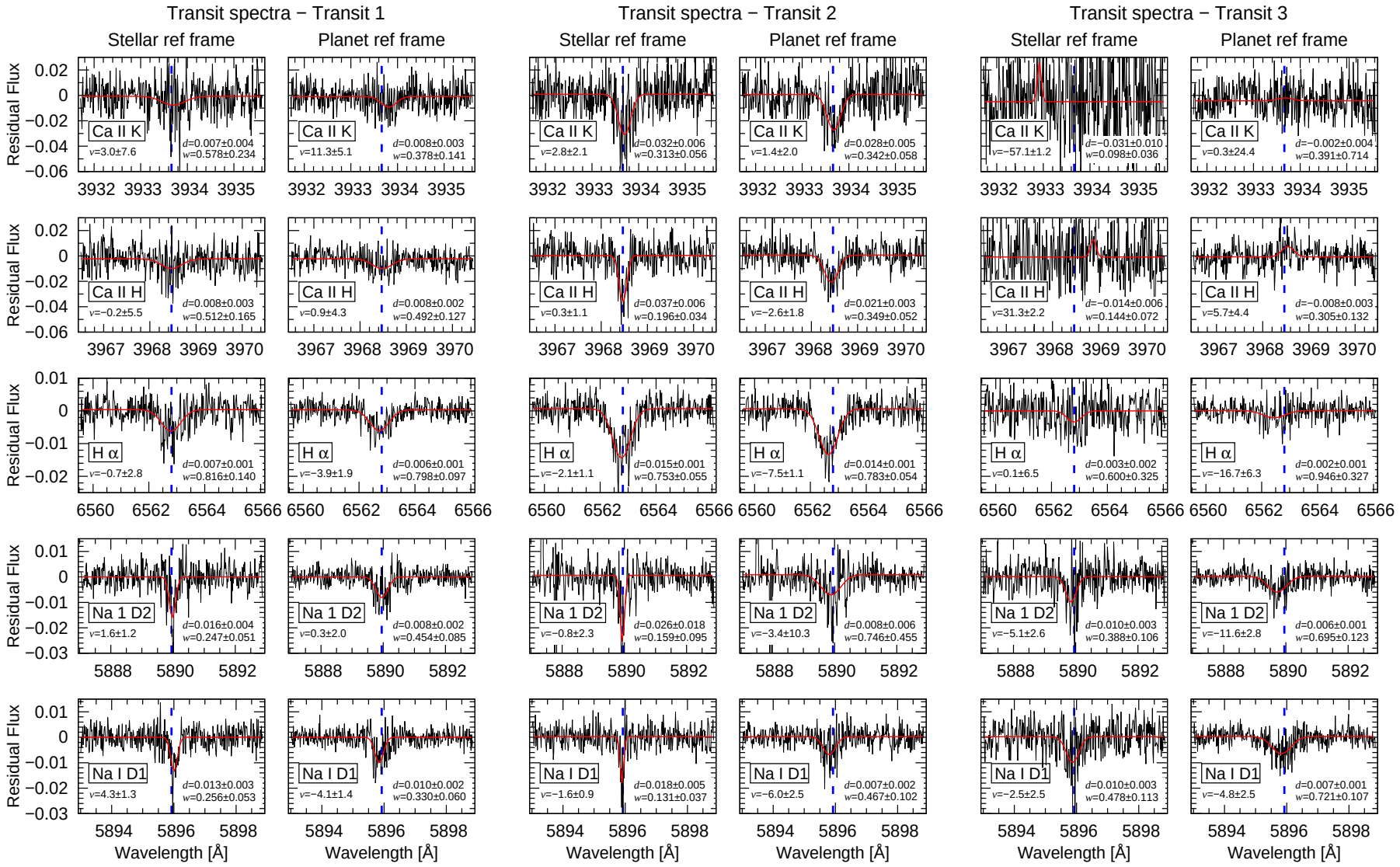

Figure . Residual Ca II H & K, Hα and Na I D1 & D2 line profiles during transit for each of Transits 1 - 3. The line profiles for the left column on each night are aligned in the stellar reference frame, while the profiles in the right columns are in the planet reference frame. The residual IT spectra are calculated by subtracting the appropriate mean OOT spectra for each line, on a night-by-night basis. The dashed line/blue indicates the rest wavelength of each line. Gaussian fits to each of the profiles over the plotted ranges are shown by the solid/red line. The Gaussian velocity shift relative to the rest wavelength, v (kms^{-1}), width, w (kms^{-1}), and depth, d, are shown in each panel.

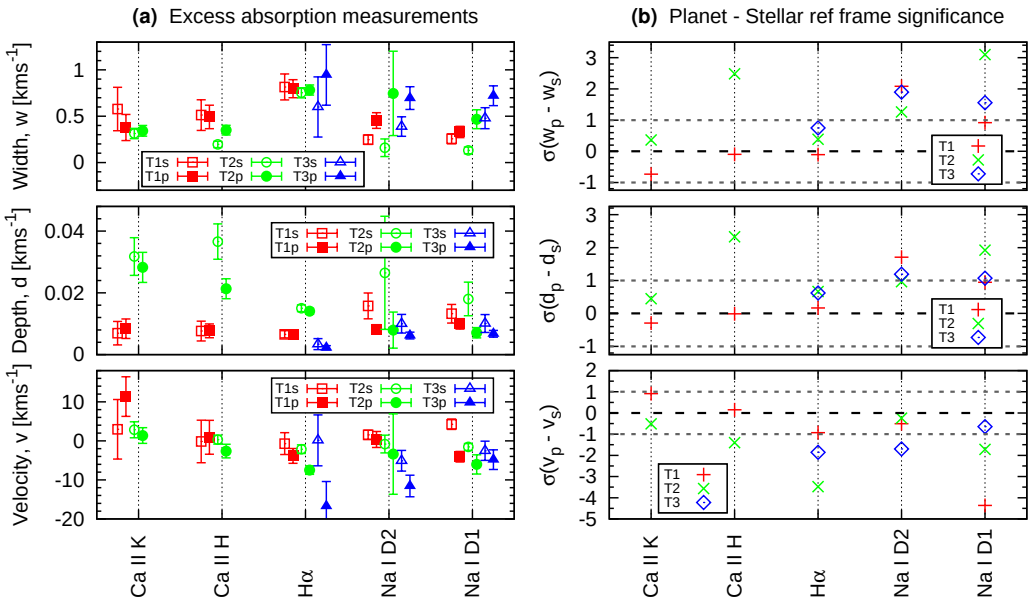

Figure 10. (a) The transit spectra depth, d, width, w (km s^{-1}), and velocity shift, v (km s^{-1}), are shown for each line, Ca II H & K, Hα and Na I D1 & D2, and for each Transit 1 - 3 in the stellar (labelled T1s - T3s, open symbols) and planet (labelled T1p - T3p, closed symbols) reference frames. The Ca II H & K points for Transit 3 are not plotted. Right panels: The difference between the measurement of each parameter in the planet reference frame minus the stellar frame as the significance determined from the uncertainties in the measurements. The zero significance (long dashed) and $\pm1\sigma$ (short dashed) levels are plotted.

mental effects. On the face of it, the simple procedure of using continuum regions on either side of the line seems reasonable as it is able to provide the precision needed to detect the apparent excess absorption with significance. This is a doubly differential method of transmission spectroscopy where first the line is compared with nearby continuum regions and then the IT and OOT spectra are differenced. We postulate this method can lead to either spurious transit signatures, or at least systematically biased transit signatures. We might similarly expect that space-based measurements, although free from ground-based atmospheric effects, would be susceptible to chromospheric variability. However passbands of typically a few hundred Å that include continuum and photospheric lines have typically been employed in space-based observations, thereby diluting the chromospheric contribution, which is confined to narrow line cores.

The problem with normalisation lies with the assumption that the flux in the continuum and the flux in the line cores arise from the same region of the star. This is obviously not the case in the strong lines we are interested in, which all contain a chromospheric emission component. The adopted continuum regions used for normalisation arise in the stellar photosphere, although they also include weaker photospheric lines, especially in the densely populated wavelength regions of Ca II H & K. The transit index measurement (Equations 3 & 4) is therefore only strictly applicable to lines that arise from a similar part of the atmosphere to the continuum regions, and even then only for an immaculate, unspotted photosphere. If HD 189733b possesses active regions confined to specific areas of the star, the transit index measurement may appear to show excess absorption during the transit, since blocking any active regions that contribute to the line core emission creates a larger contrast effect than blocking the photosphere (c.f. Chapter 5 of Haswell 2010).

In chromospherically sensitive lines such as HD 189733b, where log R'_{HK} exceeds solar maximum by 0.35 dex in log R'_{HK} (a factor of 2.2), active regions are thus likely to interfere with calculation of the light curves. Starspot corrections are generally required for broadband transmission spectrophotometry (Pont et al. 2008; Sing et al. 2011), but starspot effects may be more localised to instances where the planet transit crosses spots. Active regions, producing chromospheric emission may effect transit light curves in a similar way, but the chromospheric component in line cores probably systematically affects the whole transit lightcure depth. This can be seen clearly in the HD 189733 Ca II H & K and Hα light curves that show a deeper Transit 2 compared with Transit 1. he cores in each line studied here are also sensitive to different regions of the chromosphere and show different sensitivities to flares and other transients. Our analysis of the Na I D1 & D2 lines shows variability, but in fact Transit 2 is *less deep* than Transits 1 & 3, although the results agree within the uncertainties. Wyttenbach et al. (2015) also find variable transit depths in Na I D1 & D2, measuring 0.00339 ± 0.00057 for Transit 1, 0.00143 ± 0.00059 for Transit 2 and 0.00457 ± 0.00066 for Transit 3. Our results for Na I D1 & D2 are thus consistent with Wyttenbach et al. (2015) except for the Transit 2 measurement. The evidence for variability, *due specifically to chromospheric variability* in the Na I D1 & D2 cores, is thus less clear than for Ca II H & K and Hα, and may be the result of lower sensitivity of the Na I D1 & D2 lines to chromospheric activity.

One explanation for the very slight excess emission we

find during IT phases for the photospheric Ca I 6122 Å line might be the presence of cool starspots (e.g. see Pont et al. 2008) associated with active regions on HD 189733. The eclipsing of starspots could explain the greater degree of emission seen during Transit 2. Sing et al. (2011) find corrections for starspots, that are variable from transit to transit, of order 1 per cent (an order of magnitude greater than the precision of their transit depth measurements) are necessary for HD 189733b. The shallower transit we see in Na I D1 & D2 may therefore also be partially due to the presence of cool starspots. Variability in the Na lines could thus arise from both photospheric starspots and chromospheric plage regions.

It is also possible that we have detected the centre-to-limb variation (CLV) due to limb-darkening of the stellar disk and changes in the line profile shapes as a function of limb angle. Both the Na I D1 & D2 and Ca I light curves in Fig. 6 show marginal evidence for a bump in the transit region, with a morphology similar to that modelled and found observationally by Czesla et al. (2015). For HD 189733b transits, Czesla et al. (2015) found CLV in regions *around* the Na I D1 & D2 cores at the few $\times 10^{-3}$ level (unfortunately the core regions were excluded owing to a flaring event during those observations). In addition, the CLV of the earth in strong solar lines was investigated by Yan et al. (2015) by taking spectra of the eclipsed moon. They demonstrated that for the Earth-Sun transits, the effect is more pronounced if narrow passbands are adopted when calculating the transit curves. This is important because studies that assert that the excess absorption signal is planetary in origin, find the strongest absorption in the narrow core regions of the Na I D1 & D2 lines. The magnitude of the CLV, specifically in the core regions of strong absorption lines, clearly requires further investigation in stars such as HD 189733 with close orbiting gas giant planets.

6.2 Ca II H & K vs Hα chromospheric signatures

The observation of deep transit signatures from Ca II H & K may be explained by contrast effects, since chromospheric emission in the Ca II H & K cores is stronger as a fraction of nearby continuum flux than in Hα and Na I D1 & D2. Livingston et al. (2007) showed that a correlation exists between chromospheric emission in Ca II H & K and other lines, including Hα, during the solar cycle. The amplitude of variability in Ca II H & K was found to be stronger than in Hα. This was also shown in Fig. 1 of Meunier & Delfosse (2009), which demonstrates that Ca II H & K core emission is an order of magnitude more variable than Hα across a solar magnetic cycle. Ca II H & K and Hα are also affected by different phenomena and do not arise from the same region of the chromosphere (e.g. see Vernazza et al. 1981 and review by Hall 2008). While both Ca II H & K and Hα arise from plage regions, Hα is also more sensitive to absorption from filaments, potentially reducing the observed line core emission. With greater core emission in Ca II H & K and a higher degree of variability between quieter and more active periods on the Sun, we would thus expect to see both deeper apparent transits and more variability in Ca II H & K than in Hα. The extent to which the solar observations can be extrapolated to a more active K star such as HD 189733 is uncertain. Significant scatter was found in similar correlations in a sample of FGK and M stars, following earlier suggestions that such correlations exist (Cincunegui et al. 2007 and references therein).

6.3 Excess absorption velocities

The excess absorption seen during transit also shows variable velocity offsets. This has been interpreted as winds in the upper atmosphere of HD 189733b with estimates up to ~ 8 km s^{-1} (Wyttenbach et al. 2015). Louden & Wheatley (2015) used the Transit 3 data to spatially resolve the Na absorption, reporting winds on the leading and trailing limb of the planet, which they interpreted as an eastward equatorial jet. However, we detect a transient increase in line core flux in Ca II H & K and Hα during Transit 3, probably the result of a small flare. This means it is likely that any putative planetary wind measurements will be severely affected by chromospheric/coronal transients. Our time series spectra in Fig. 8 (e) indicate excess absorption aligned in the stellar reference frame during Transit 3, with velocities of -5.1 ± 2.6 km s^{-1} (Na I D1) and -2.5 ± 2.5 km s^{-1} (Na I D2) (Figs. 5.2.1 & 10). We conclude the putative planetary wind signature in fact arises in the dynamic behaviour of the outer layers of the stellar atmosphere.

7 SUMMARY & CONCLUSION

We have detected excess absorption in the Ca II H & K lines of HD 189733 during transit of its close orbiting giant exoplanet. We also detected excess absorption in Hα, and re-examined previous results for Na I D1 & D2. The transit depths are significantly variable in Ca II H & K and Hα, with Transit 2 exhibiting the strongest line absorption. We studied the time series spectra of each line during the three transits and find evidence that the excess absorption is located in the stellar reference frame. We postulate that the chromosphere of HD 189733 is the dominant contributor to the excess transit absorption and responsible for its variable nature since the flux measured in the cores of the lines we have studied contains a significant chromospheric contribution. A systematic affect is introduced because for any given transit, the chromospheric emission will be slightly different, and localised to specific regions on the stellar surface, whereas the continuum emission used for normalisation originates in the stellar photosphere. Temporal variability (from one transit to the next) in chromospheric emission will lead to changes in the depth of the apparent absorption, while localised systematic effects, where the planet transits active regions, will also result in variability. The Na I D1 & D2 lines core are less sensitive to chromospheric variability than Ca II H & K and Hα and may contain systematics from both chromospheric features such as plage and filaments, and photospheric variability from starspots.

Observations aimed at detecting specific lines in the atmospheres of transiting exoplanets with ground-based observations thus likely yield systematically biased transit signatures if the lines being probed are sensitive to stellar chromospheric emission. Space-based observations can, in principle, measure the flux time series for all observed wavelengths so that (singly) differential transmission spectroscopy reveals the difference between IT and OOT spectra. In practice

however, often the OOT spectra are used to remove systematic effects, or detrending is necessary (Pont et al. 2007) so even space-based transmission spectroscopy may be affected by this systematic bias when observing chromospherically sensitive regions (Pont et al. 2013). It is worth noting also that since active regions vary in time, the issue is likely to be more important for planet hosting stars with higher activity levels, such as HD 189733.

Our analysis shows that multiple transits and careful scrutiny of time series spectra are desirable to assess the nature of excess absorption during exoplanetary transits. It would be interesting to obtain further transit observations of both HD 189733 and HD 209458 in combination with long term activity monitoring. Study of Ca II H & K is both difficult and risky because it requires that the star be active, with sufficient line reversal flux to obtain reliable transit light curves. HD 189733 is the most favourable target for study of Ca II H & K transit effects; even HD 209458, being much less active, does not possess significant Ca II H & K line core flux. The Na I D1 & D2 and Hα lines occur in regions with better continuum flux and thus offer the potential to investigate transit and stellar activity effects on a wider sample of systems.

ACKNOWLEDGMENTS

J.R.B. and C.A.H. were supported by the STFC under the grant ST/L000776/1. D.S. was supported by an STFC studentship. We would like to thank the anonymous referee for reading and providing constructive feedback to help improve the manuscript.

REFERENCES

Agol E., Cowan N. B., Knutson H. A., Deming D., Steffen J. H., Henry G. W., Charbonneau D., 2010, ApJ, 721, 1861
Astudillo-Defru N., Rojo P., 2013, A&A, 557, A56
Barman T., 2007, ApJ, 661, L191
Barnes J. R., et al., 2012, MNRAS, 424, 591
Boisse I., et al., 2009, A&A, 495, 959
Bouchy F., et al., 2005, A&A, 444, L15
Cauley P. W., Redfield S., Jensen A. G., Barman T., Endl M., Cochran W. D., 2015, ApJ, 810, 13
Charbonneau D., Brown T. M., Latham D. W., Mayor M., 2000, ApJ, 529, L45
Charbonneau D., Brown T. M., Noyes R. W., Gilliland R. L., 2002, ApJ, 568, 377
Cincunegui C., Díaz R. F., Mauas P. J. D., 2007, A&A, 469, 309
Claret A., 2000, A&A, 363, 1081
Clough S. A., Iacono M. J., Moncet J. L., 1992, J. Geophys. Res., 97, 15761
Clough S. A., W. S. M., Mlawer E. J., Delamere J. S., Iacono M. J., Cady-Pereira K., Boukabara S., Brown P., 2005, J. Quant. Spectrosc. Radiat. Transfer, 91, 233
Collier Cameron A., Horne K., Penny A., Leigh C., 2002, MNRAS, 330, 187
Collier Cameron A., Bruce V. A., Miller G. R. M., Triaud A. H. M. J., Queloz D., 2010, MNRAS, 403, 151
Czesla S., Klocová T., Khalafinejad S., Wolter U., Schmitt J. H. M. M., 2015, A&A, 582, A51
Eastman J., Gaudi B. S., Agol E., 2013, PASP, 125, 83
Fortney J. J., Sudarsky D., Hubeny I., Cooper C. S., Hubbard W. B., Burrows A., Lunine J. I., 2003, ApJ, 589, 615
Fortney J. J., Shabram M., Showman A. P., Lian Y., Freedman R. S., Marley M. S., Lewis N. K., 2010, ApJ, 709, 1396
Fossati L., et al., 2010, ApJ, 714, L222
Fossati L., Ayres T. R., Haswell C. A., Bohlender D., Kochukhov O., Flöer L., 2013, ApJ, 766, L20
Fuhrmeister B., Lalitha S., Poppenhaeger K., Rudolf N., Liefke C., Reiners A., Schmitt J. H. M. M., Ness J.-U., 2011, A&A, 534, A133
Hall J. C., 2008, Living Reviews in Solar Physics, 5
Haswell C. A., 2010, Transiting Exoplanets. Cambridge University Press, 2010. ISBN: 9780521139380
Haswell C. A., et al., 2012, ApJ, 760, 79
Henry G. W., Marcy G. W., Butler R. P., Vogt S. S., 2000, ApJ, 529, L41
Jenkins J. S., et al., 2006, MNRAS, 372, 163
Kramida A., Reader J., Ralchenko Y., NIST ASD Team 2015, Online: http://physics.nist.gov/asd, Online: http://physics.nist.gov/asd
Lagrange A., Desort M., Meunier N., 2010, A&A, 512, A38+
Lecavelier Des Etangs A., Vidal-Madjar A., Désert J.-M., Sing D., 2008, A&A, 485, 865
Livingston W., Wallace L., White O. R., Giampapa M. S., 2007, ApJ, 657, 1137
Lodders K., 1999, ApJ, 519, 793
Louden T., Wheatley P. J., 2015, ApJ, 814, L24
Meunier N., Delfosse X., 2009, A&A, 501, 1103
Noyes R. W., Hartmann L., Baliunas S. L., Duncan D. K., Vaughan A. H., 1984, ApJ, 279, 763
Pont F., et al., 2007, A&A, 476, 1347
Pont F., Knutson H., Gilliland R. L., Moutou C., Charbonneau D., 2008, MNRAS, 385, 109
Pont F., Sing D. K., Gibson N. P., Aigrain S., Henry G., Husnoo N., 2013, MNRAS, 432, 2917
Rauscher E., Marcy G. W., 2006, PASP, 118, 617
Redfield S., Endl M., Cochran W. D., Koesterke L., 2008, ApJ, 673, L87
Seager S., 2003, in Deming D., Seager S., eds, Astronomical Society of the Pacific Conference Series Vol. 294, Scientific Frontiers in Research on Extrasolar Planets. pp 457–466 (arXiv:astro-ph/0305338)
Seager S., Mallén-Ornelas G., 2003, ApJ, 585, 1038
Seager S., Sasselov D. D., 2000, ApJ, 537, 916
Shkolnik E., Walker G. A. H., Bohlender D. A., 2003, ApJ, 597, 1092
Shkolnik E., Bohlender D. A., Walker G. A. H., Collier Cameron A., 2008, ApJ, 676, 628
Sing D. K., et al., 2011, MNRAS, 416, 1443
Sing D. K., et al., 2012, MNRAS, 426, 1663
Sing D. K., et al., 2016, Nature, 529, 59
Snellen I. A. G., Albrecht S., de Mooij E. J. W., Le Poole R. S., 2008, A&A, 487, 357
Torres G., Winn J. N., Holman M. J., 2008, ApJ, 677, 1324
Triaud A. H. M. J., et al., 2009, A&A, 506, 377
Vaughan A. M., Preston G. W., Wilson O. C., 1978, PASP, 90, 267
Vernazza J. E., Avrett E. H., Loeser R., 1981, ApJS, 45, 635
Winn J. N., et al., 2006, ApJ, 653, L69
Winn J. N., et al., 2007, AJ, 133, 1828
Wright J. T., Marcy G. W., Butler R. P., Vogt S. S., 2004, ApJS, 152, 261
Wyttenbach A., Ehrenreich D., Lovis C., Udry S., Pepe F., 2015, A&A, 577, A62
Yan F., Fosbury R. A. E., Petr-Gotzens M. G., Zhao G., Pallé E., 2015, A&A, 574, A94
Zechmeister M., Anglada-Escudé G., Reiners A., 2014, A&A, 561, A59

This paper has been typeset from a TEX/LATEX file prepared by the author.